energies

MDPI

*Article*

# Effect of Biochars Derived from Different Feedstocks on Methane Production Kinetics and Microbial Community Dynamics in Anaerobic Digestion of Food Wastewater

**Sang-Yoon Kim [1,2], Young-Seob Yu [3], Chang-Suk Jin [3], Kiwook Kwon [4], Gui-Seck Bae [2] and Chang-Hyun Kim [1,*]**

[1] School of Animal Life Convergence Science, Hankyong National University, Anseong 17579, Republic of Korea; tkddbs8524@naver.com
[2] Biogas Research Center, Hankyong National University, Anseong 17579, Republic of Korea; gsbae@hknu.ac.kr
[3] KEC System Co., Ltd., Hwaseong 18244, Republic of Korea; u0seob@naver.com (Y.-S.Y.); csjinfj@hanmail.net (C.-S.J.)
[4] Environmental Technology Division, Korea Testing Laboratory, Seoul 08389, Republic of Korea; kwkwon@ktl.re.kr
* Correspondence: kimch@hknu.ac.kr; Tel.: +82-010-9257-6608

## Abstract

Anaerobic digestion of food wastewater (FW) is a sustainable avenue for renewable biogas production; however, high-level accumulation of volatile fatty acids (VFAs) frequently compromises its operational stability. Although biochar amendment has emerged as a promising strategy to mitigate acid stress by facilitating direct interspecies electron transfer (DIET), there is a fundamental knowledge gap regarding the governing roles of its physical specific surface area (SSA) versus chemical carbon properties. In our study, we evaluated five biochars derived from distinct feedstocks (wood chips, wood pellets, chicken manures, coffee grounds, and rice husks) pyrolyzed at 350 °C in a FW anaerobic digestion system at a dosage of 1% (*w*/*v*) over a 68-day digestion period. Biochemical methane potential (BMP) assays were combined with modified Gompertz kinetic modeling and high-throughput Next-Generation Sequencing (NGS). Despite wood pellet biochar exhibiting an overwhelmingly superior multi-point Brunauer–Emmett–Teller (BET) SSA (179.97 $m^2/g$) due to pelletization-induced micropores (<2 nm), its maximum methane production rate ($R_m$ = 18.40 mL/day) showed negligible kinetic enhancement compared to the Control (18.47 mL/day). This discrepancy was attributed to steric hindrance, which physically restricts anaerobic microorganisms (0.5–2.0 µm) from accessing the internal macroporous network. Conversely, rice husk biochar, characterized by a low SSA (0.9211 $m^2/g$), the highest carbon content (80.62%), and the lowest oxygen ratio (6.63%), achieved the highest biochemical methane yield ($B_u$ = 0.380 $Nm^3$/kg-$VS_{added}$) and peak methane production rate ($R_m$ = 20.79 mL/day, a 12.6% increase over the Control). It also shortened the time to reach the peak production rate ($t_0$) from 2.68 to 2.53 days. In NGS community profiling, rice husk biochar promoted syntrophic associations by enriching *Syntrophaceticus* (10.17%), while *Methanosarcina* remained the predominant methanogen across all treatments (90.99–95.71%). Our findings indicate that physical SSA alone does not dictate methane kinetics rather, a balance of macroporous accessibility and carbon matrix properties supports syntrophic methanogenesis. To design high-efficiency, biochar-assisted anaerobic digesters, our study provides critical insights into the selection strategy for biochar feedstocks based on chemical carbon properties.

**Keywords:** anaerobic digestion; food wastewater; biochar; direct interspecies electron transfer (DIET); microbial community dynamics

Check for updates

Academic Editors: Chengyan Wen and Haiyong Wang

Received: 1 October 2026
Revised: 20 October 2026
Accepted: 17 November 2026
Published: 19 November 2026

**Copyright:** © 2026 by the authors. Licensee MDPI, Basel, Switzerland. This article is an open access article distributed under the terms and conditions of the Creative Commons Attribution (CC BY) license.

## 1. Introduction

Anaerobic digestion is a sustainable and environmentally friendly energy-conversion technology. It simultaneously processes organic waste and produces methane-based biogas [1,2]. However, the stability of this process is easily compromised when treating wastewater (FW) from food waste with high concentrations of both soluble organic matter and solids [3]. While the initial hydrolysis and acidogenesis stages of FW anaerobic digestion proceed rapidly, a high level of volatile fatty acids (VFAs) can accumulate when the reaction rate of methanogenesis fails to keep pace [3,4]. This accumulation of VFAs causes digester pH, severely inhibiting pH-sensitive methanogen activity and reducing overall process efficiency, leading to system failure [4,5]. To overcome these instabilities and maximize methane conversion efficiency, global research has focused on activating the direct interspecies electron transfer (DIET) mechanism between microorganisms [6,7]. In traditional anaerobic metabolic pathways, interspecies hydrogen transfer (IHT) mediated by chemical vectors, such as $H_2$ or formate, has been dominant [6]. However, its electron transfer rate is inherently limited because IHT relies on strict thermodynamic equilibrium conditions between hydrogen-producing and hydrogen-consuming reactions [6,8]. Conversely, DIET directly exchanges electrons between syntrophic acetogens and methanogens through conductive materials. This dramatically accelerates electron transfer rates compared with IHT and maximizes methane production kinetics [7,8]. Consequently, activating DIET via conductive carbon materials has recently gained substantial interest as a thermodynamic bypass to alleviate volatile fatty acid accumulation during food-waste digestion [9].

Biochar, a carbonaceous material produced by biomass pyrolysis under oxygen-limited conditions, has attracted significant attention in anaerobic digestion as both a physical immobilization matrix—owing to its porous architecture and specific surface area (SSA) [10,11]—and an electron-mediating carrier capable of stimulating DIET through its carbon skeleton and surface functional groups [11,12]. The physicochemical properties of biochar vary substantially with feedstock source (e.g., lignocellulosic wood, agricultural residues, or livestock manure) and production conditions [10,13]. Previous studies indicate that lignocellulosic biochars typically exhibit higher carbonization and aromatic matrix development than mineral-rich manure biochars [13,14]. However, among plant-derived materials, the extent of carbon network development and surface heteroatom distribution varies substantially depending on the native precursor structure and thermal transformation behavior [13].

Although recent investigations have explored biochar-assisted anaerobic digestion systems [15,16] and comparative feedstock evaluations [9,17], the relative contributions of physical pore accessibility (SSA) versus the degree of carbonization remain insufficiently understood, particularly in high-solid food wastewater (FW) systems prone to rapid VFA accumulation and severe acid stress [16]. Clear kinetic elucidation is needed to determine whether a structure with maximized physical SSA or one with a high degree of carbonization is more effective in activating DIET within microbial communities adapted to food wastewater [12,16].

Therefore, this study investigated five distinct biochars derived from different feedstocks (wood chips, wood pellets, chicken manures, coffee grounds, and rice husks) synthesized at 350 °C. This relatively low pyrolysis temperature was selected to represent an energy-efficient and economically viable production threshold for practical waste valorization. This threshold preserves functional surface heteroatoms and redox-active moieties capable of mediating interspecies electron transfer before extensive high-temperature graphitization [18–20]. We evaluated the quantitative impacts of each biochar's elemental composition and BET SSA on cumulative methane yield and production rates. Furthermore, the modified Gompertz model was used to derive kinetic parameters, including lag-phase

reduction and maximum methane production rates [21]. We hypothesized that under the severe organic acid stress of food wastewater digestion, microbial access to macropores and carbon matrix properties would more critically facilitate syntrophic kinetics than physical BET surface area dominated by inaccessible micropores. Through this approach, we aim to identify the optimal biochar feedstock characteristics to maximize food wastewater anaerobic digestion efficiency and establish an academic foundation for designing high-efficiency, stable biochar-assisted processes.

## 2. Materials and Methods

### *2.1. Substrate and Inoculum*

We collected FW as the substrate in our study in April 2024 from a commercial food-waste-recycling facility in Icheon, Republic of Korea. The collected FW was immediately transported to the laboratory, homogenized, and stored at 4 °C in a cold room before characterization and reactor inoculation to prevent premature biological degradation and acidification. The chemical composition and physicochemical properties of the collected FW are detailed in Table 1. The initial concentrations of total solids (TS) and volatile solids (VS) in the FW were measured at 100,497 mg/L and 87,505 mg/L, respectively.

**Table 1.** Chemical composition of food wastewater.

| Parameter | | Food Wastewater |
|---|---|---|
| Ph | | 3.52 |
| TS [1] (mg/L) | | 100,497 |
| VS [2] (mg/L) | | 87,505 |
| TKN [3] (mg/L) | | 3854 |
| $NH_4^+$-N [4] (mg/L) | | 305 |
| $COD_{Cr}$ [5] (mg/L) | | 153,635 |
| $SCOD_{Cr}$ [6] (mg/L) | | 106,769 |
| TVFAs [7] (mg/L as acetate) | | 11,777 |
| Theoretical methane potential (Bth) ($Nm^3$/kg-$VS_{added}$) | | 0.506 |
| Elemental composition (wt.%, d.b. [8]) | C | 45.25 |
| | H | 6.44 |
| | O [9] | 34.60 |
| | N | 3.35 |
| | S | 0.00 |

All data correspond to the average value of three replicate measures ($n = 3$). [1] Total solids; [2] volatile solids; [3] total Kjeldahl nitrogen; [4] ammonium nitrogen; [5] chemical oxygen demand; [6] soluble chemical oxygen demand; [7] total volatile fatty acids; [8] dry basis; [9] oxygen content was calculated by difference: O (%) = 100 − (C + H + N + S).

### *2.2. Preparation and Characterization of Biochars*

Our study investigated five distinct biochars derived from different feedstocks. The raw biomass materials were collected from specific sources: wood chips from recycled timber, wood pellets from softwood, chicken manures from a broiler poultry farm, coffee grounds from a commercial coffee processing facility, and rice husks from a local rice processing complex. All biochar samples were synthesized via pyrolysis in a sealed, box-type muffle furnace under oxygen-limited conditions. The furnace was heated at a constant rate of 5 c/min from ambient temperature to the target temperature of 350 °C and held isothermally for 2 h. The threshold temperature of 350 °C was specifically designated based on the minimum temperature requirement for biochar carbonization [10,22], thereby minimizing energy consumption and maximizing process feasibility for practical biochar production. A scanning electron microscope was used to examine surface morphological

features and porous microstructures (SEM; MIRA3, TESCAN, Brno, Czech Republic) at an acceleration voltage of 10.0 kV. An elemental analyzer quantitatively determined the elemental composition (C, H, O, N, and S) (EA1108, Thermo Finnigan LLC, San Jose, CA, USA) [22,23] (Table 2).

**Table 2.** Elemental composition of biochars derived from different feedstocks.

| Parameter | | Wood Chips | Wood Pellets | Chicken Manures | Coffee Grounds | Rice Husks |
|---|---|---|---|---|---|---|
| Elemental composition (wt.%, d.b. [1]) | C | 70.03 | 72.15 | 31.30 | 54.57 | 80.62 |
| | H | 3.58 | 1.74 | 2.07 | 2.80 | 1.90 |
| | O | 20.97 | 11.06 | 18.21 | 11.76 | 6.63 |
| | N | 0.74 | 0.61 | 3.45 | 1.03 | 3.48 |
| | S | 0.00 | 0.00 | 0.89 | 0.00 | 0.00 |
| O/C molar ratio | | 0.22 | 0.12 | 0.44 | | 0.16 |

All data corresponds to the average value of three replicate measures ($n = 3$). [1] Dry basis. Oxygen (O) was calculated by difference. Note: The elemental analyzer measures the combustible organic fraction (C, H, N, S), while mineral silica and inorganics are accounted for in the ash content.

The SSA and micro/mesoporous structural features of the biochars were analyzed with nitrogen ($N_2$) gas adsorption–desorption isotherms, using an automated surface area and porosity analyzer (ASAP 2020, Micromeritics Instrument Corp., Norcross, GA, USA) [23,24]. Prior to $N_2$ physisorption measurements, the samples were thoroughly degassed under vacuum at 105 °C for 24 h to evacuate residual moisture and surface-bound volatile impurities [23,24]. The SSA values were derived according to the Brunauer–Emmett–Teller (BET) equation within the relative pressure range ($p/p_0$) of 0.05 to 0.35 [24,25]. To ensure high analytical accuracy and reliability regarding micropore accessibility, we implemented both single-point BET (at relative pressures corresponding to monolayer coverage) and multi-point BET methods [25,26].

### *2.3. Biochemical Methane Potential (BMP) Test*

The BMP assays were conducted following standardized analytical guidelines [27]. Batch anaerobic reactors were used under mesophilic conditions (38 °C) to evaluate the BMP values of the unamended Control and experimental treatments, supplemented with biochar materials as conductive additives.

In accordance with the standard methods for examining water and wastewater, the general physicochemical parameters of the substrate, inoculum, and digestate were determined, including total solids (TS), volatile solids (VS), chemical oxygen demand ($COD_{Cr}$), soluble chemical oxygen demand ($SCOD_{Cr}$), total Kjeldahl nitrogen (TKN), ammonium nitrogen ($NH_4^+$-N), alkalinity, and total volatile fatty acids (TVFAs).

The anaerobic inoculum was harvested from a 20 L mesophilic (38 °C) plug-flow reactor (PFR) operated at Hankyong National University. The reactor was fed with FW at a hydraulic retention time (HRT) of 30 days. Before initiating the BMP assays, the harvested inoculum was pre-incubated under mesophilic anaerobic conditions for 14 days to exhaust the remaining endogenous organic matter and minimize background biogas production, in accordance with standard degassing protocols [27,28]. Although this pre-incubation step lowered the inoculum vs. concentration (4.85 g/L; Table 3), an adequate microbial-to-substrate balance without organic shock overload was maintained by strictly fixing the substrate-to-inoculum (S/I) ratio at 0.7 on a vs. basis. Batch experiments were performed in 250 mL serum bottles containing 160 mL of the pre-incubated inoculum; food wastewater was added as the substrate. To stimulate DIET through conductive additives, five distinct biochars derived from wood chips, wood pellets, chicken manures, coffee

grounds, and rice husks were used at a 1% dosage ($w/v$, DM) relative to the total working volume. Prior to setup, all biochar samples were oven-dried at 105 °C for 24 h and stored in a desiccator. We established an unamended Control group lacking biochar and operated a blank group containing only inoculum to calibrate background methane generation. Background methane production from the inoculum-only blank averaged 1.07 mL, and this was subtracted from the total methane yield of all treatment bottles to calculate the substrate's net methane production. All experimental conditions, including the blank, were performed in triplicate. The reactor headspace was thoroughly purged with high-purity $N_2$ gas to remove residual oxygen. After this, the bottles were sealed tightly using blue butyl rubber stoppers and aluminum crimp caps to ensure complete anaerobiosis. The batch mixtures were incubated at 38 °C in a convection incubator with manual daily agitation over a total digestion period of 68 days.

**Table 3.** Chemical composition of inoculum.

| Parameter | Inoculum |
|---|---|
| pH | 7.78 |
| TS [1] (mg/L) | 10,049 |
| VS [2] (mg/L) | 4852 |
| TKN [3] (mg/L) | 1827 |
| $NH_4^+$-N [4] (mg/L) | 1095 |
| CODCr [5] (mg/L) | 33,344 |
| SCODCr [6] (mg/L) | 21,610 |
| TVFAs [7] (mg/L as acetate) | 1816 |
| Alkalinity (as $CaCO_3$) | 7683 |

All data correspond to the average value of three replicate measures ($n = 3$). [1] Total solids; [2] volatile solids; [3] total Kjeldahl nitrogen; [4] ammonium nitrogen; [5] chemical oxygen demand; [6] soluble chemical oxygen demand; [7] total volatile fatty acids.

The theoretical methane potential was calculated stoichiometrically using Boyle's (1976) stoichiometric equation [29] (Equation (1)) based on the measured elemental composition (C, H, O, N) of the food wastewater substrate in Table 1. Based on the complete stoichiometric reaction of organic matter, the theoretical methane potential (Bth) was calculated using Equation (2):

$$\begin{gathered} C_a\,H_b\,O_c\,N_d\,S_e + (a - \tfrac{b}{4} - \tfrac{c}{2} + \tfrac{3d}{4} + \tfrac{e}{2})H_2O \\ \rightarrow \left(\tfrac{a}{2} + \tfrac{b}{8} - \tfrac{c}{4} - \tfrac{3d}{8} - \tfrac{e}{4}\right) CH_4 + \left(\tfrac{a}{2} - \tfrac{b}{8} + \tfrac{c}{4} + \tfrac{3d}{8} + \tfrac{e}{4}\right) CO_2 + dNH_3 + eH_2S \end{gathered} \quad (1)$$

$$B_{th}(Nm^3kg^{-1} - VS_{added}) \;=\; 22.4 \times \left[\frac{(4a + b - 2c - 4d - 2e)/8}{12a + b + 16c + 14d + 32e}\right] \quad (2)$$

The total volume of generated biogas was measured using a water column gas volume meter, and the volumetric methane fraction ($CH_4$) was quantified via GC-TCD. The volume of generated methane was determined by multiplying the measured biogas volume by the corresponding methane percentage. Subsequently, this was converted to dry gas volume at standard temperature and pressure (0 °C, 1 atm) using Equation (3), where $V_{drygas}$ is the volume of dry gas under standard conditions (0 °C, 1 atm); T is the operating temperature of the reactor; $V_{\text{wet gas at T °C}}$ is the volume of wet gas at the operating temperature of the reactor (T, 38 °C); P is the atmospheric pressure at the time the volume of the gas was measured; and $P_T$ is the saturated water vapor pressure (mmHg) at T°C. In this study, P was 760 mmHg, and $P_T$ was calculated as the saturated water vapor pressure at 38 °C [21,30].

$$V_{dry\ gas} \;=\; V_{wet\ gas\ T°C} \times \frac{273}{(273 + T)} \times \frac{(P - P_T)}{760} \quad (3)$$

The progress of cumulative methane production [31] was interpreted with the modified Gompertz model (Equation (4)), which enabled the optimization of cumulative methane production data using these equations [32]. In particular, the modified Gompertz model was applied to estimate the lag-phase time and maximum methane production rate, where $M_t$ is the cumulative amount of methane production (mL), t is the anaerobic fermentation time (days), P is the final methane production (mL), e is the exponential component, Rm is the maximum methane production rate (mL/day), and λ represents the lag growth phase time (days).

$$M_t = P \times \exp\{-\exp[\frac{R_m \cdot e}{P}(\lambda - t) + 1]\} \quad (4)$$

To assess the statistical accuracy and robustness of the kinetic regression, the goodness of fit was evaluated using the coefficient of determination ($R^2$) and the root mean square error (RMSE). Values closer to 1.0 and a lower RMSE represented higher model fidelity.

### *2.4. Microbial Community Analysis*

At the end of the 68-day anaerobic digestion period, for each experiment, digestate samples were harvested from the triplicate serum bottles of each treatment and pooled in equal volumes to generate a representative composite sample. Genomic DNA (gDNA) was extracted from 0.25 g of the homogenized digestate using the DNeasy PowerSoil Pro Kit (Qiagen, Hilden, Germany) according to the manufacturer's instructions. The concentration and purity of the extracted gDNA were confirmed using a NanoDrop spectrophotometer (Thermo Fisher Scientific, Waltham, MA, USA).

The V3 and V4 hypervariable regions of the 16S rRNA gene were amplified using universal primer pairs containing Illumina adapter overhang sequences: forward primer 341F (5′-TCGTCGGCAGCGTCAGATGTGTATAAGAGACAGCCTACGGGNGGCWGCAG-3′) and reverse primer 805R (5′-GTCTCGTGGGCTCGGAGATGTGTATAAGAGACAGGACTACHVGGGTATCTAATCC-3′). The input gDNA (2 ng) was PCR-amplified with a 5 × reaction buffer, 1 mM dNTP mix, 500 nM of each primer, and Herculase II fusion DNA polymerase (Agilent Technologies, Santa Clara, CA, USA). The reaction conditions for the first PCR cycle were as follows: initial heat activation at 95 °C for 3 min; 25 cycles of denaturation at 95 °C for 30 s, annealing at 55 °C for 30 s; and extension at 72 °C for 30 s. This was followed by a final extension at 72 °C for 5 min. The PCR products were purified using AMPure XP beads (Agencourt Bioscience, Beverly, MA, USA). Subsequent index PCR was performed using Nextera XT Indexed Primers (Illumina, San Diego, CA, USA) for 10 cycles. The finalized libraries were quantified via qPCR using the KAPA Library Quantification Kit (Roche, Basel, Switzerland) and qualified with a TapeStation D1000 ScreenTape (Agilent Technologies, Waldbronn, Germany). Paired-end sequencing (2 × 300 bp) was executed on the Illumina MiSeq™ platform through Macrogen Inc. (Seoul, Republic of Korea). Raw sequence reads were processed through the QIIME2 pipeline (v2022.2) with DADA2 for quality filtering, denoising, and amplicon sequence variant (ASV) generation. Taxonomic classification of Bacteria and Archaea was assigned against the SILVA reference database (release 138). To evaluate the community structure, archaeal ASVs were retrieved and independently normalized to 100% relative abundance.

### *2.5. Analytical Methods for Biogas Composition*

Using a gas chromatograph (Clarus 680, PerkinElmer, Waltham, MA, USA) equipped with a thermal conductivity detector (TCD), the volumetric composition of the generated biogas was quantified. A Hayesep Q packed column (3 mm ID × 3 m length, 80–100 mesh size) was used to perform gas separation. High-purity argon (Ar) served as the carrier gas at a constant flow rate of 30 mL/min. The operational temperatures for the sample injector,

column oven, and TCD were set at 150 °C, 90 °C, and 150 °C, respectively, in accordance with standardized biogas chromatography guidelines [27].

### *2.6. Statistical Analysis*

The statistical analysis of the experimental parameters ($B_u$, BD, $R_m$, and $t_0$) was performed using the general linear model (GLM) procedure of the software package SAS® (SAS ver. 9.4, SAS Institute Inc., Cary, NC, USA). Tukey's honestly significant difference (HSD) test at a significance level of $p < 0.05$ was applied to evaluate pairwise differences among treatment means [33].

For high-throughput NGS microbial community profiling, sequencing reads obtained from representative pooled composite samples were quantified and compared based on relative taxonomic abundance (%).

### *2.7. Use of Artificial Intelligence Tools*

During the preparation of this manuscript, the authors utilized an AI-assisted language and bibliographic tool solely for English language refinement, stylistic editing, and citation formatting. Following the use of this tool, the authors thoroughly reviewed, audited, and verified all the cited literature against original primary sources with active DOIs, and take full responsibility for the integrity and accuracy of the publication. The AI tool was not used to generate, collect, analyze, or interpret any experimental data, nor did it influence the scientific study design or conclusions.

## 3. Results and Discussion

### *3.1. Physicochemical Characteristics, Specific Surface Area (SSA), and Surface Morphology of Biochars*

We analyzed the physicochemical properties, elemental composition, and structural features of biochars derived from different feedstocks (wood chips, wood pellets, chicken manures, coffee grounds and rice husks) to evaluate their functional roles as additives in anaerobic digestion of FW (Tables 2 and 4 and Figure 1).

The elemental analysis showed significant variations in carbon (C), nitrogen (N), hydrogen (H), and oxygen (O) contents among feedstocks (Table 2). Biochars derived from lignocellulosic biomass exhibited high carbon contents: rice husks (80.62%), wood chips (70.03%), and wood pellets (72.15%). By contrast, the nutrient-rich nature of animal manure was reflected in the chicken manure biochar, which showed a low carbon content (31.30%) and elevated nitrogen (3.45%) and sulfur (0.89%) levels.

The SSA of biochars was determined using both single-point and multi-point BET methods (Table 4). While the single-point BET provides a rapid estimation of total surface area based on gas adsorption at a fixed relative pressure ($p/p_0 = 0.3$), the multi-point BET method accounts for monolayer–multilayer adsorption dynamics across a broader relative pressure range ($0.05 \leq p/p_0 \leq 0.30$) to yield a more rigorous and scientifically robust measurement for porous materials. According to the multi-point BET evaluation, the wood pellet biochar exhibited an exceptionally high SSA of 179.97 $m^2/g$, whereas other biochars showed substantially lower values: chicken manures (4.04 $m^2/g$), rice husks (0.92 $m^2/g$), wood chips (0.41 $m^2/g$), and coffee grounds (0.35 $m^2/g$). Scanning electron microscopy (SEM) further supported these structural observations (Figure 1). Consistent with its elevated SSA, the wood pellet biochar developed extensive microporosity through the thermal devolatilization of compacted softwood fibers during pyrolysis. In contrast, wood chips displayed tubular vascular channels, coffee grounds showed irregular macroporous cavities, and rice husks exhibited a longitudinally grooved, layered fibrous epidermal architecture.

**Table 4.** Specific surface area of different biochars calculated by single-point and multi-point BET.

| Biochar | Specific Surface Area ($m^2/g$) | |
|---|---|---|
| | **Single-Point BET** | **Multi-Point BET** |
| Wood chips | 0.3840 | 0.4096 |
| Wood pellets | 176.9794 | 179.97 |
| Chicken manures | 3.8451 | 4.0401 |
| Coffee grounds | 0.2504 | 0.3536 |
| Rice husks | 0.7984 | 0.9211 |

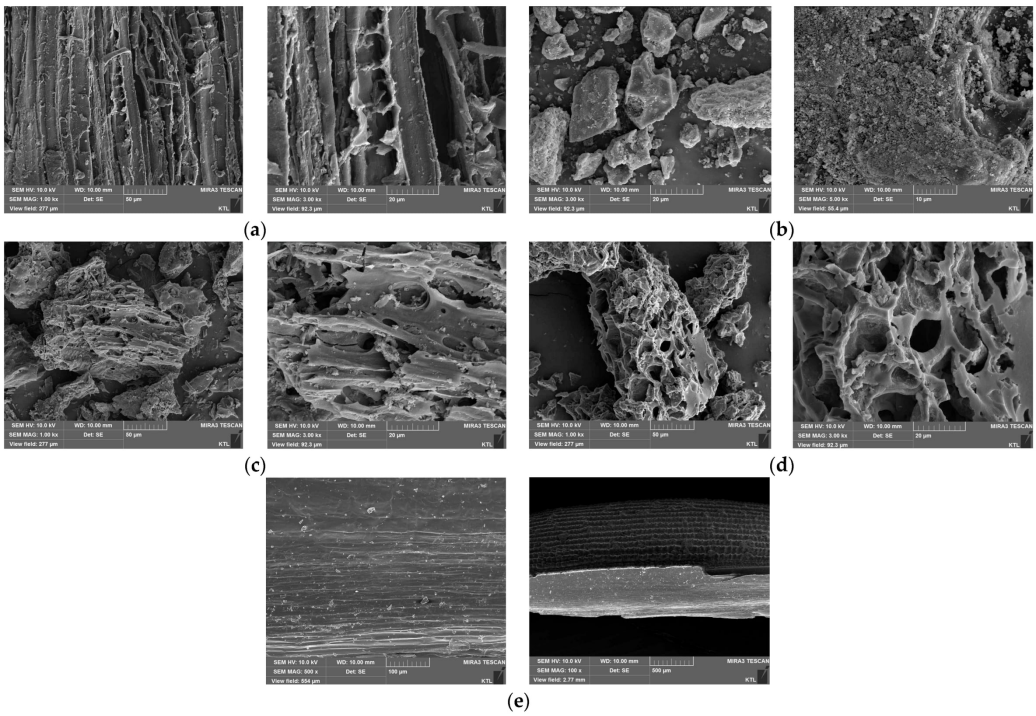



**Figure 1.** Scanning electron microscopy (SEM) images illustrating the surface morphology and porous structures of biochars derived from various feedstocks: (**a**) wood chips; (**b**) chicken manures; (**c**) wood pellets; (**d**) coffee grounds; and (**e**) rice husks.

The unique physical architecture and chemical composition of the rice husk biochar provide a favorable matrix environment for anaerobic consortia. Specifically, the grooved outer surface and fibrous layers observed in Figure 1e offer accessible external physical contact sites for microbial colonization, free from the steric pore-exclusion constraints observed in micropore-dominated materials [34]. Regarding elemental properties, the high relative carbon content (80.62%) and low O/C molar ratio (0.06) reflect an extensively condensed carbon matrix with reduced oxygenated surface polarity. In the anaerobic digestion literature, such carbonaceous characteristics are frequently linked to enhanced electron-mediating potential [8,35]. Rather than acting merely as an inert physical adsorbent, the rice husks biochar may provide a biocompatible surface that supports syntrophic associations between acetate-oxidizing bacteria and methanogenic archaea [8,17].

Furthermore, although the ash content was not directly quantified in this study, the inherent mineral composition of the feedstocks likely influenced the digestion dynamics based on the previous literature. As shown in Table 2, chicken manure biochar has a low carbon content (31.30%) and elevated nitrogen (3.45%) and sulfur levels (0.89%). This is consistent with the mineral- and ash-rich nature of livestock manure biochars reported in previous studies [13,14]. While these inorganic minerals provide essential trace nutrients,

excessive release of organic nitrogen and sulfur during initial hydrolysis can contribute to localized free ammonia and sulfide stress, providing a plausible explanation for the prolonged time to reach the maximum production rate ($t_0$ = 3.03 days, Table 5). In contrast, plant-derived rice husk biochar is well documented in the literature to retain an amorphous biogenic silica ($SiO_2$) skeleton [10,13], providing rigid structural integrity that resists mechanical degradation during mixing while maintaining accessible outer contact surfaces without toxic metal inhibition.

**Table 5.** Biochemical methane potential ($B_u$), anaerobic biodegradability (BD), maximum methane production rate ($R_m(t_0)$), time to reach maximum production rate ($t_0$), and model goodness of fit indices ($R^2$, RMSE) in food wastewater anaerobic digestion amended with different biochars.

| Parameters | $B_u$ [1] | BD [2] | $R_m(t_0)$ [3] | $t_0$ [4] | $R^2$ [6] | RMSE [7] |
|---|---|---|---|---|---|---|
| | $Nm^3/kg\text{-}VS_{added}$ | % | mL/Day | Day | | mL |
| Control | 0.342 [c] | 67.6 [c] | 18.47 [b] | 2.68 [bc] | 0.986 | 3.44 |
| Wood chips | 0.363 [b] | 71.7 [b] | 19.50 [ab] | 2.63 [bc] | 0.984 | 3.94 |
| Wood pellets | 0.357 [b] | 70.6 [b] | 18.40 [b] | 2.76 [b] | 0.979 | 4.40 |
| Chicken manures | 0.362 [b] | 71.5 [b] | 18.35 [b] | 3.03 [a] | 0.986 | 3.69 |
| Coffee grounds | 0.360 [b] | 71.1 [b] | 19.27 [ab] | 2.61 [bc] | 0.989 | 3.29 |
| Rice husks | 0.380 [a] | 75.1 [a] | 20.79 [a] | 2.53 [c] | 0.986 | 3.86 |
| *p*-value | <0.0001 | <0.0001 | 0.0071 | 0.0004 | - | - |
| SEM [5] | 0.0029 | 0.5292 | 0.4295 | 0.0542 | - | - |

[1] Biochemical methane potential; [2] biodegradability ($B_u$/Bth × 100%); [3] maximum methane production rate; [4] date of reaching maximum methane production rate; [5] standard error mean; [6] coefficient of determination; [7] root mean square error. [abc] Means with different superscripts within the same column differ significantly ($p < 0.05$) according to Tukey's honestly significant difference (HSD) test.

### *3.2. Methane Yield and Reaction Kinetics of Biochars*

Over a 68-day incubation period, we evaluated different biochar additives and their effects on methane yield and degradation kinetics during anaerobic digestion of FW using BMP tests (Table 5 and Figure 2).

As illustrated in Figure 2, all biochar-amended digesters and the Control showed rapid initial methane generation during the first 10 days, followed by a plateau phase. Based on the elemental composition of the food wastewater (Table 1), the theoretical stoichiometric methane potential (Bth) was calculated as 0.506 $Nm^3/kg\text{-}VS_{added}$. The unamended Control digester yielded an ultimate $B_u$ of 0.342 $Nm^3/kg\text{-}VS_{added}$, corresponding to an anaerobic biodegradability (BD) of 67.6% (Table 5), with a maximum methane production rate ($R_m$) of 18.47 mL/day reached at $t_0$ = 2.68 days. Biochar supplementation generally enhanced biomethanation performance, with $B_u$ values increasing to 0.357–0.380 $Nm^3/kg\text{-}VS_{added}$ and biodegradability improving to 70.6–75.1% across all treatments ($p < 0.05$). Among all tested biochars, rice husk biochar achieved the highest performance, demonstrating an ultimate $B_u$ of 0.380 $Nm^3/kg\text{-}VS_{added}$ (BD = 75.1%; an 11.1% increase over the Control; $p < 0.05$), a peak $R_m$ of 20.79 mL/day (a 12.6% increase over the Control; $p < 0.05$), and the shortest $t_0$ of 2.53 days ($p < 0.05$).

Wood chip (0.363 $Nm^3/kg\text{-}VS_{added}$), chicken manure (0.362 $Nm^3/kg\text{-}VS_{added}$), and coffee ground (0.360 $Nm^3/kg\text{-}VS_{added}$) biochars also moderately improved methane yield and biodegradability ($p < 0.05$, Table 5). Notably, chicken manure biochar had the longest time to peak production rate ($t_0$ = 3.03 days, $p < 0.05$), likely due to its elevated nitrogen (3.45%) and sulfur (0.89%) contents (Table 2). This could lead to localized free ammonia or sulfide accumulation and temporarily prevent methanogenic initiation. In contrast, wood pellet biochar resulted in a statistically significant increase in ultimate yield ($B_u$ = 0.357 $Nm^3/kg\text{-}VS_{added}$, BD = 70.6%; $p < 0.05$) compared to the Control, suggesting beneficial organic ad-

sorption or trace buffering capacity; however, its maximum kinetic rate ($R_m$ = 18.40 mL/day, $t_0$ = 2.76 days) showed no significant kinetic acceleration over the Control.

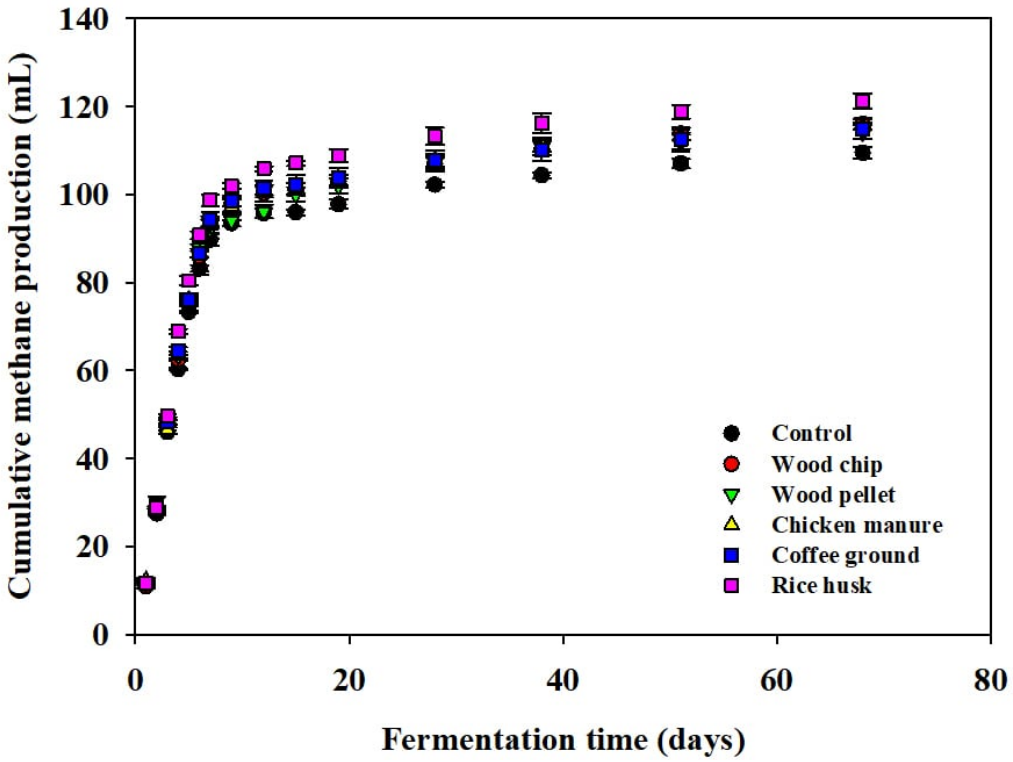



**Figure 2.** Cumulative methane production curves over 68 days during the anaerobic digestion of food wastewater amended with different biochars (data points represent net cumulative methane production after subtracting the inoculum-only blank; error bars indicate standard deviations of triplicate reactors, $n$ = 3).

The modified Gompertz model showed exceptional statistical accuracy in describing cumulative methane production dynamics across all experimental groups, as evidenced by high coefficients of determination ($R^2$ = 0.979–0.989) and low root mean square error values (RMSE = 3.29–4.40 mL) (Table 5). This robust agreement demonstrates that the non-linear kinetic model accurately captured both the rapid exponential methane production during the initial 10 days and the subsequent asymptotic plateau phase, validating the derived $R_m$ and $t_0$ as reliable kinetic benchmarks.

From a reaction kinetics perspective, rice husk biochar' superiority—evidenced by its highest $R_m$ and shortest $t_0$—indicates the accelerated syntrophic conversion of accumulated VFAs into methane during the early acidogenic stage [8]. The reduction in $t_0$ (2.53 days) effectively alleviates kinetic bottlenecks during the lag phase [15,36]. This kinetic facilitation is attributed to (1) the longitudinally grooved, layered fibrous epidermal architecture outer shell and layered fibrous structure, which provide accessible physical scaffolding for rapid microbial colonization and biofilm formation [11,34], and (2) the favorable carbon matrix properties and surface redox-active functional groups that potentially facilitate direct interspecies electron transfer (DIET) between syntrophic acetate-oxidizing bacteria and methanogens, bypassing the thermodynamic constraints of interspecies hydrogen diffusion [8,36].

This complementary dual-route mechanism alleviates the thermodynamic constraints of conventional IHT by supporting early VFA conversion [31,33]. Furthermore, while biochar alkalinity can contribute to localized acid mitigation, the inoculum's high baseline alkalinity (7683 mg/L for $CaCO_3$, as shown in Table 3) maintained stable pH buffering

across all treatments, indicating that rice husk biochar's kinetic superiority was driven by syntrophic bio-electrochemical interactions rather than bulk chemical neutralization alone. Consequently, this microbial shift corresponds with the shortened $t_0$ and elevated $R_m$ observed uniquely in the rice husk biochar treatment.

### *3.3. Microbial Community Structure and Interspecies Electron Transfer Mechanisms*

To clarify the biological mechanisms underlying the kinetic enhancements and $B_u$ improvements induced by biochars, we conducted high-throughput NGS to analyze archaeal and bacterial community structures at both the phylum and genus levels.

In the archaeal community, Methanobacteriota was the primary phylum across all digesters (>98.23%), with Thermoplasmatota at 0.97–1.75% (Figure 3a). At the genus level, *Methanosarcina* dominated all treatments and accounted for 90.99–95.71% of total archaeal sequences (Figure 3b). *Methanosarcina* has membrane-bound c-type cytochromes; thus, it is a mixotrophic methanogen capable of operating through acetoclastic, hydrogenotrophic, and DIET pathways [2,8].

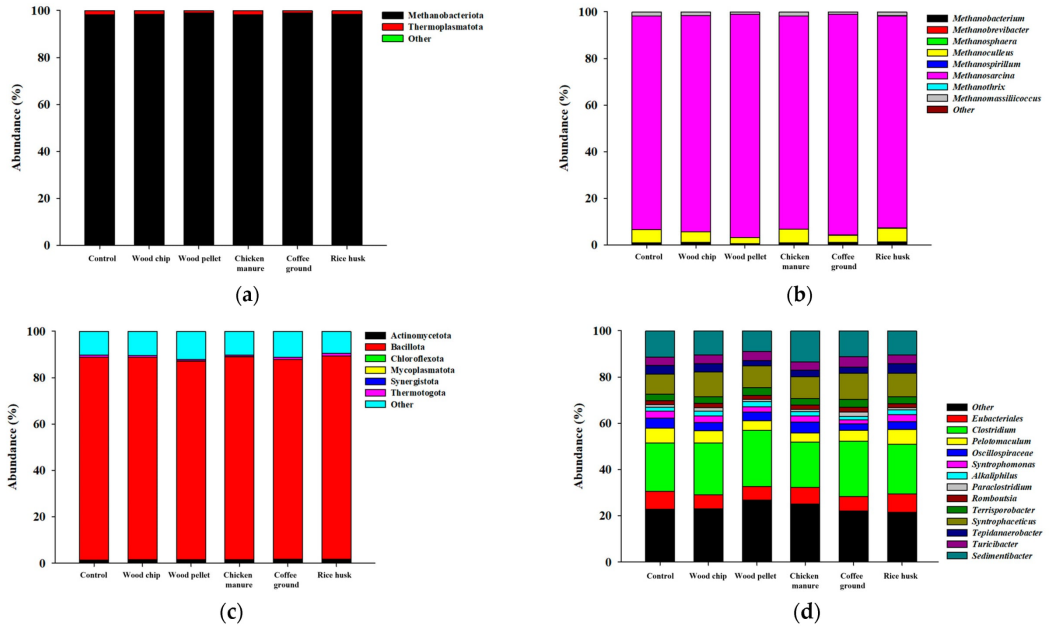



**Figure 3.** Relative abundance of microbial communities at the phylum and genus levels during food wastewater anaerobic digestion amended with different biochars: archaeal community at the (**a**) phylum and (**b**) genus levels; bacterial community at the (**c**) phylum and (**d**) genus levels.

When evaluating archaeal shifts alongside the BMP performance (Table 5), the relative abundance of the hydrogenotrophic genus *Methanoculleus* provides meaningful insight into process kinetics. In the Control, *Methanoculleus* maintained 5.56%. In the rice husk treatment that achieved the highest methane yield and maximum production rate, *Methanoculleus* remained at 5.92%. By contrast, in low-performing biochars, such as wood pellet, its abundance decreased to 2.56%.

This difference helps explain the kinetic performance observed in the rice husk treatment. While *Methanosarcina* served as the primary terminal methanogen across all reactors (90.99–95.71%), its preservation in the rice husk treatment directly indicated active complementary dual-pathway methanogenesis. In this cooperative framework, potential solid-state electron transfer via *Methanosarcina* was complemented by hydrogenotrophic methanogenesis via *Methanoculleus* to scavenge residual dissolved $H_2$ and sustain thermodynamically favorable syntrophy [1,9]. Conversely, in the wood pellet treatment, the marked reduction

in *Methanoculleus* (2.56%) reflects a disrupted syntrophic balance, aligning with its inability to improve kinetic parameters compared to the Control.

In the bacterial community, Bacillota (85.70–87.62%) formed the major phylum, followed by Actinomycetota (1.38–1.70%) and Thermotogota (0.62–1.05%) (Figure 3c). At the genus level, the primary bacterial framework responsible for breaking down complex organic compounds into VFAs comprised hydrolytic and acidogenic fermenters, predominantly represented by *Clostridium* (19.61–24.48%) and *Sedimentibacter* (8.90–13.55%), along with *Pelotomaculum* (4.13–6.48%) (Figure 3d).

Notably, the relative abundance of *Syntrophaceticus*, an obligate syntrophic acetate-oxidizing bacterium (SAOB), showed a distinct association with biochar addition [33]. Compared to the Control (8.68%), an elevated abundance of *Syntrophaceticus* was detected across biochar treatments, reaching 11.48% in coffee ground, 10.63% in wood chip, and 10.17% in rice husk digesters. While accelerated acidogenesis generates high acetate flux that drives *Syntrophaceticus* proliferation [36], substrate availability alone cannot thermodynamically sustain acetate oxidation without continuous removal of evolved electrons or hydrogen [37]. Indeed, despite harboring higher *Syntrophaceticus* abundances, coffee ground and wood chip digesters achieved lower peak $R_m$ than the rice husk biochar (Table 5). This kinetic discrepancy indicates that substrate availability was secondary to downstream electron-transfer coupling. This was uniquely facilitated by the accessible fibrous architecture and carbon matrix of the rice husk biochar together with *Methanosarcina* (90.99%) and *Methanoculleus* (5.92%) [38].

Under high VFA loading conditions, conventional acetate oxidation coupled with hydrogenotrophic methanogenesis via IHT is thermodynamically constrained unless hydrogen partial pressure remains exceptionally low [39,40]. The concurrent presence of *Syntrophaceticus* (10.17%), *Methanosarcina* (90.99%), and *Methanoculleus* (5.92%) in the rice husk biochar treatment is hypothesized to support an integrated syntrophic network. Here, the accessible grooved fibrous architecture and favorable carbonization of rice husk biochar provide physical contact sites that potentially facilitate direct or mediated interspecies electron transfer (DIET) to *Methanosarcina*, and *Methanoculleus* simultaneously consumes residual hydrogen [8,31]. This complementary dual-route mechanism alleviates the thermodynamic constraints of conventional IHT by supporting early VFA conversion [31,33], consistent with the shortened $t_0$ and elevated $R_m$ observed uniquely in the rice husk biochar treatment.

This complementary dual-route mechanism alleviates the thermodynamic constraints of conventional IHT by supporting early VFA conversion [31,33], consistent with the shortened $t_0$ and elevated $R_m$ observed uniquely in the rice husk biochar treatment. Importantly, this microbial reconfiguration represents a productive functional adaptation rather than a chemical stress response to biochar leachates (e.g., residual phenolics or dissolved silica). In anaerobic systems, chemical toxicity characteristically prolongs the lag phase and suppresses methanogenesis. In contrast, rice husk biochar had the shortest $t_0$, the highest $R_m$, and superior biodegradability, confirming that the pre-conditioned biochar (dried at 105 °C) did not exert inhibitory chemical stress, but instead fostered a kinetically advantageous syntrophic consortium.

## 4. Conclusions and Limitations

### *4.1. Scope, Limitations, and Future Perspectives*

While this study provides valuable comparative insights into feedstock-specific biochar properties and anaerobic digestion kinetics, several methodological boundaries and limitations should be acknowledged:

(1) Direct Electrochemical Measurements: Bulk electrical conductivity, cyclic voltammetry, and electron exchange capacity (EEC) were not directly quantified on the biochar samples

due to material constraints. Therefore, the enhanced interspecies electron transfer (DIET) pathway discussed herein remains an evidence-based hypothesis supported by microbial community shifts and the literature, rather than direct electrochemical confirmation.

(2) Experimental Boundaries: The evaluations were conducted in batch mesophilic BMP assays at a single biochar dosage (1% $w/v$) and a single low pyrolysis temperature (350 °C). Although 350 °C was established as the temperature at which to evaluate an energy-efficient threshold with preserved surface redox functionalities, pyrolyzing feedstocks across a broader temperature gradient (e.g., 350–700 °C) would be valuable to systematically delineate the transition from surface functional group-mediated electron transfer to graphitic matrix conduction.

(3) Control Assays: A dedicated biochar-only blank and an inert bicarbonate buffer control were not operated in parallel. Although the literature confirms that minimal volatile gas release occurs in biochars at 350 °C and the inoculum maintained high inherent alkalinity, future studies should isolate pure chemical buffering from solid-state electron transfer.

(4) Future Research: Long-term continuous or semi-continuous anaerobic digesters (e.g., CSTR or UASB) should be investigated to determine biochar retention, shear resistance, and microbial biofilm stability under dynamic loading. Metatranscriptomic sequencing and conductive atomic force microscopy (C-AFM) are recommended to provide direct biophysical proof of solid-state electron transfer networks.

### *4.2. Conclusions*

This study evaluated five distinct biochars derived from different feedstocks (wood chips, wood pellets, chicken manures, coffee grounds, and rice husks) pyrolyzed at 350 °C to elucidate their functional impacts on methane production kinetics and microbial consortium dynamics in food wastewater anaerobic digestion. Contrary to the common assumption that high physical surface area drives kinetic acceleration, our findings indicate that physical specific surface area (SSA) alone does not govern methane production kinetics. The wood pellet biochar has an exceptionally high multi-point BET SSA (179.97 $m^2/g$); however, its kinetic enhancement remained negligible as steric hindrance restricted anaerobic microorganisms (0.5–2.0 μm) from accessing internal sub-2 nm micropores.

Instead, macro-structural accessibility and carbonization characteristics proved more critical factors under organic acid stress. The rice husk biochar, characterized by a longitudinally grooved fibrous outer surface, the highest carbon content, and the lowest O/C molar ratio, achieved the highest biochemical methane yield, peak production rate, and the shortest time to peak production rate. Metagenomic profiling revealed that successful kinetic performance was supported by a balanced syntrophic consortium comprising enriched *Syntrophaceticus* (10.17%) alongside predominant *Methanosarcina* (90.99%) and preserved hydrogenotrophic *Methanoculleus* (5.92%). This provides evidence of an active dual-pathway syntrophic network.

Overall, these findings demonstrate that when selecting biochar additives for high-strength organic wastewater treatment, accessible surface architecture and carbon matrix properties provide greater kinetic benefits than micropore-dominated physical surface area. These insights provide a practical foundation for selecting cost-effective biochar feedstocks to alleviate volatile fatty acid inhibition and enhance operational stability in anaerobic digestion systems.

**Author Contributions:** Conceptualization: C.-H.K. and S.-Y.K.; data curation: C.-H.K. and S.-Y.K.; formal analysis: S.-Y.K., G.-S.B. and C.-H.K.; methodology: C.-H.K. and S.-Y.K.; software: S.-Y.K.; validation: C.-H.K., S.-Y.K., Y.-S.Y., C.-S.J. and K.K.; investigation: C.-H.K. and S.-Y.K.; writing—original draft: S.-Y.K.; writing: C.-H.K. and S.-Y.K. All authors have read and agreed to the published version of the manuscript.

**Funding:** This research was supported by the Agriculture and Food Convergence Technologies Program for Research Manpower Development (RS-2024-00400922) and the Korea Institute of Energy Technology Evaluation and Planning (KETEP) grant funded by the Korean government (MOTIE) (Project No. 2021202090056A) partly supported this work.

**Institutional Review Board Statement:** Not applicable.

**Informed Consent Statement:** Not applicable.

**Data Availability Statement:** The raw data supporting the conclusions of this article will be made available by the authors upon reasonable request.

**Acknowledgments:** The authors would like to express their sincere appreciation to all those who provided technical assistance, supported the experiments, and contributed to sample collection and laboratory work. During the preparation of this work, the authors utilized an AI-assisted language tool (Gemini, Google LLC) solely for English phrasing assistance and bibliographic formatting. After using this tool, the authors independently audited all contents and take full responsibility for the final content of the publication.

**Conflicts of Interest:** Authors Young-Seob Yu and Chang-Suk Jin were employed by the company KEC System Co., Ltd. The remaining authors declare that the research was conducted in the absence of any commercial or financial relationships that could be construed as a potential conflict of interest.

## References

1. Appels, L.; Baeyens, J.; Degrève, J.; Dewil, R. Principles and potential of the anaerobic digestion of waste-activated sludge. *Prog. Energy Combust. Sci.* **2008**, *34*, 755–781. [CrossRef]
2. Weiland, P. Biogas production: Current state and perspectives. *Appl. Microbiol. Biotechnol.* **2010**, *85*, 849–860. [CrossRef] [PubMed]
3. Xu, F.; Li, Y.; Ge, X.; Yang, L.; Li, Y. Anaerobic digestion of food waste—Challenges and opportunities. *Bioresour. Technol.* **2018**, *247*, 1047–1058. [CrossRef] [PubMed]
4. Franke-Whittle, I.H.; Walter, A.; Ebner, C.; Insam, H. Investigation into the effect of high concentrations of volatile fatty acids in anaerobic digestion on methanogenic communities. *Waste Manag.* **2014**, *34*, 2080–2089. [CrossRef] [PubMed]
5. Ward, A.J.; Hobbs, P.J.; Holliman, P.J.; Jones, D.L. Optimisation of the anaerobic digestion of agricultural resources. *Bioresour. Technol.* **2008**, *99*, 7928–7940. [CrossRef] [PubMed]
6. Rotaru, A.-E.; Shrestha, P.M.; Liu, F.; Markovaite, B.; Chen, S.; Nevin, K.P.; Lovley, D.R. A new model for electron flow during anaerobic digestion: Direct interspecies electron transfer to Methanosaeta for the reduction of carbon dioxide to methane. *Energy Environ. Sci.* **2014**, *7*, 408–415. [CrossRef]
7. Lovley, D.R. Syntrophy Goes Electric: Direct Interspecies Electron Transfer. *Annu. Rev. Microbiol.* **2017**, *71*, 643–664. [CrossRef] [PubMed]
8. Baek, G.; Kim, J.; Cho, K.; Bae, J.; Lee, C. The biostimulation of anaerobic digestion with (semi)conductive ferric oxides: Their potential for enhanced biomethanation. *Appl. Microbiol. Biotechnol.* **2015**, *99*, 10355–10366. [CrossRef] [PubMed]
9. Ma, H.; Chen, L.; Guo, W.; Wang, L.; Zhang, J.; Zhang, D. Synergistic promotion of direct interspecies electron transfer by biochar and $Fe_3O_4$ nanoparticles to enhance methanogenesis in anaerobic digestion of vegetable waste. *Fermentation* **2024**, *10*, 656. [CrossRef]
10. Lehmann, J.; Joseph, S. *Biochar for Environmental Management: Science, Technology and Implementation*, 2nd ed.; Routledge: London, UK, 2015; pp. 1–30.
11. Luo, C.; Lu, F.; Shao, L.; He, P. Application of eco-compatible biochar in anaerobic digestion to relieve acid stress and promote the selective colonization of functional microbes. *Water Res.* **2015**, *68*, 710–718. [CrossRef] [PubMed]
12. Chen, S.; Rotaru, A.-E.; Liu, F.; Philips, J.; Woodard, T.L.; Nevin, K.P.; Lovley, D.R. Carbon cloth stimulates direct interspecies electron transfer in syntrophic co-cultures. *Bioresour. Technol.* **2014**, *173*, 82–86. [CrossRef] [PubMed]

13. Joseph, S.; Cowie, A.L.; Van Zwieten, L.; Bolan, N.; Budai, A.; Buss, W.; Cayuela, M.L.; Graber, E.R.; Ippolito, J.A.; Kuzyakov, Y.; et al. How biochar works, and when it doesn't: A review of mechanisms controlling soil and plant responses to biochar. *GCB Bioenergy* **2021**, *13*, 1731–1764. [CrossRef]
14. Leng, L.; Huang, H.; Li, H.; Li, J.; Zhou, W. Biochar stability assessment methods: A review. *Sci. Total Environ.* **2019**, *647*, 210–222. [CrossRef] [PubMed]
15. Shanmugam, S.R.; Adhikari, S.; Nam, H.; Sajib, S.K. Effect of biochar on methane generation from glucose and aqueous phase of algae liquefaction using mixed anaerobic cultures. *Biomass Bioenergy* **2018**, *108*, 479–486. [CrossRef]
16. Zhang, L.; Lim, E.Y.; Loh, K.C.; Ok, Y.S.; Lee, J.T.E.; Shen, Y.; Wang, C.H.; Dai, Y.; Tong, Y.W. Biochar enhanced thermophilic anaerobic digestion of food waste: Focusing on biochar particle size, microbial community analysis and pilot-scale application. *Energy Convers. Manag.* **2020**, *209*, 112654. [CrossRef]
17. Quintana-Najera, J.; Blacker, A.J.; Fletcher, L.A.; Ross, A.B. Understanding the Influence of Biochar Augmentation in Anaerobic Digestion by Principal Component Analysis. *Energies* **2023**, *16*, 2523. [CrossRef]
18. Shen, Y.; Yu, Y.; Zhang, Y.; Urgun-Demirtas, M.; Yuan, H.; Zhu, N.; Dai, X. Role of redox-active biochar with distinctive electrochemical properties to promote methane production in anaerobic digestion of waste activated sludge. *J. Clean. Prod.* **2021**, *278*, 123212. [CrossRef]
19. Cruz Viggi, C.; Simonetti, S.; Palma, E.; Pagliaccia, P.; Braguglia, C.; Fazi, S.; Baronti, S.; Navarra, M.A.; Pettiti, I.; Koch, C.; et al. Enhancing methane production from food waste fermentate using biochar: The added value of electrochemical testing in pre-selecting the most effective type of biochar. *Biotechnol. Biofuels* **2017**, *10*, 303. [CrossRef] [PubMed]
20. Sun, T.; Levin, B.D.A.; Guzman, J.J.L.; Enders, A.; Muller, D.A.; Angenent, L.T.; Lehmann, J. Rapid electron transfer by the carbon matrix in natural pyrogenic carbon. *Nat. Commun.* **2017**, *8*, 14873. [CrossRef] [PubMed]
21. Lay, J.J.; Li, Y.Y.; Noike, T. Mathematical model for methane production from landfill bioreactors. *J. Environ. Eng.* **1998**, *124*, 730–736. [CrossRef]
22. International Biochar Initiative (IBI). *Standardized Product Definition and Product Testing Guidelines for Biochar That Is Used in Soil*, Version 2.1; IBI: Portland, OR, USA, 2015.
23. Zheng, H.; Wang, Z.; Zhao, J.; Herbert, S.; Xing, B. Sorption of antibiotic sulfamethoxazole varies with biochars produced at different temperatures. *Environ. Pollut.* **2013**, *181*, 60–67. [CrossRef] [PubMed]
24. Thommes, M.; Kaneko, K.; Neimark, A.V.; Olivier, J.P.; Rodriguez-Reinoso, F.; Rouquerol, J.; Sing, K.S. Physisorption of gases, with special reference to the evaluation of surface area and pore size distribution (IUPAC Technical Report). *Pure Appl. Chem.* **2015**, *87*, 1051–1069. [CrossRef]
25. Brunauer, S.; Emmett, P.H.; Teller, E. Adsorption of gases in multimolecular layers. *J. Am. Chem. Soc.* **1938**, *60*, 309–319. [CrossRef]
26. Sing, K.S. Reporting physisorption data for gas/solid systems with special reference to the determination of surface area and porosity (Recommendations 1984). *Pure Appl. Chem.* **1985**, *57*, 603–619. [CrossRef]
27. Angelidaki, I.; Alves, M.; Bolzonella, D.; Borzacconi, L.; Campos, J.L.; Guwy, A.J.; Kalyuzhnyi, S.; Jenicek, P.; van Lier, J.B. Defining the biomethane potential (BMP) of solid organic wastes and energy crops: A proposed protocol for batch assays. *Water Sci. Technol.* **2009**, *59*, 927–934. [CrossRef] [PubMed]
28. Holliger, C.; Alves, M.; Andrade, D.; Angelidaki, I.; Astals, S.; Baier, U.; Bougrier, C.; Buffière, P.; Carballa, M.; de Wilde, V.; et al. Towards a standardization of biomethane potential tests. *Water Sci. Technol.* **2016**, *74*, 2515–2522. [CrossRef] [PubMed]
29. Boyle, W.C. Energy recovery from sanitary landfills—A review. In *Microbial Energy Conversion*; Schlegel, H.G., Barnea, J., Eds.; Pergamon Press: Oxford, UK, 1976; pp. 119–138.
30. Oh, S.-Y.; Yoon, Y.-M. Energy recovery efficiency of poultry slaughterhouse sludge cake by hydrothermal carbonization. *Energies* **2017**, *10*, 1876. [CrossRef]
31. Luna-delRisco, M.; Normak, A.; Orupõld, K. Biochemical methane potential of different organic wastes and energy crops from Estonia. *Agron. Res.* **2011**, *9*, 331–342.
32. Sørensen, A.H.; Winther-Nielsen, M.; Ahring, B.K. Kinetics of lactate, acetate and propionate in unadapted and lactate-adapted thermophilic, anaerobic sewage sludge: The influence of sludge adaptation for start-up of thermophilic UASB-reactors. *Appl. Microbiol. Biotechnol.* **1991**, *34*, 823–827. [CrossRef]
33. Tukey, J.W. Comparing individual means in the analysis of variance. *Biometrics* **1949**, *5*, 99–114. [CrossRef]
34. Cai, J.; He, P.; Wang, Y.; Shao, L.; Lü, F. Effects and optimization of the use of biochar in anaerobic digestion of food wastes. *Waste Manag. Res.* **2016**, *34*, 409–416. [CrossRef] [PubMed]
35. Johnravindar, D.; Patria, R.D.; Lee, J.T.E.; Zhang, L.; Tong, Y.W.; Wang, C.-H.; Ok, Y.S.; Kaur, G. Syntrophic interactions in anaerobic digestion: How biochar properties affect them. *Sustain. Environ.* **2021**, *7*, 1945282. [CrossRef]
36. Westerholm, M.; Müller, B.; Singh, A.; Schnürer, A. Growth Characteristics and Thermodynamics of Syntrophic Acetate Oxidizers. *Environ. Sci. Technol.* **2019**, *53*, 5512–5520. [CrossRef] [PubMed]
37. Dolfing, J. Thermodynamic Constraints on Syntrophic Acetate Oxidation. *Appl. Environ. Microbiol.* **2014**, *80*, 1539–1540. [CrossRef] [PubMed]

38. Rotaru, A.-E.; Calabrese, F.; Stryhanyuk, H.; Musat, F.; Shrestha, P.M.; Weber, H.S.; Snoeyenbos-West, O.L.; Lovley, D.R.; Richnow, H.H.; Musat, N. Conductive Particles Enable Syntrophic Acetate Oxidation between Geobacter and Methanosarcina from Coastal Sediments. *mBio* **2018**, *9*, e00226-18. [CrossRef] [PubMed]
39. Zhao, Z.; Zhang, Y.; Woodard, T.L.; Nevin, K.P.; Lovley, D.R. Enhancing syntrophic metabolism in up-flow anaerobic sludge blanket reactors with conductive carbon materials. *Bioresour. Technol.* **2015**, *191*, 140–145. [CrossRef] [PubMed]
40. Westerholm, M.; Moestedt, J.; Schnürer, A. Biogas production through syntrophic acetate oxidation and deliberate operating strategies for improved digester performance. *Appl. Energy* **2016**, *179*, 124–135. [CrossRef]

**Disclaimer/Publisher's Note:** The statements, opinions and data contained in all publications are solely those of the individual author(s) and contributor(s) and not of MDPI and/or the editor(s). MDPI and/or the editor(s) disclaim responsibility for any injury to people or property resulting from any ideas, methods, instructions or products referred to in the content.